analytical chemistry

Article

pubs.acs.org/ac

Toward Biocompatible Nuclear Hyperpolarization Using Signal Amplification by Reversible Exchange: Quantitative *in Situ* Spectroscopy and High-Field Imaging

Jan-Bernd Hövener,*[,†,‡,§] Niels Schwaderlapp,[‡] Robert Borowiak,[†,‡,§] Thomas Lickert,[‡] Simon B. Duckett,[∥] Ryan E. Mewis,[∥] Ralph W. Adams,[∥] Michael J. Burns,[∥] Louise A. R. Highton,[∥] Gary G. R. Green,[∥] Alexandra Olaru,[∥] Jürgen Hennig,[‡] and Dominik von Elverfeldt[‡]

[†]German Consortium for Cancer Research (DKTK), Heidelberg, Germany

[‡]Medical Physics, Department of Radiology, University Medical Center Freiburg, 79098 Freiburg, Germany

[§]German Cancer Research Center (DKFZ), Heidelberg, Germany

[∥]Centre for Hyperpolarisation in Magnetic Resonance, University of York, York, YO10 5DD, U.K.

ABSTRACT: Signal amplification by reversible exchange (SABRE) of a substrate and *para*hydrogen at a catalytic center promises to overcome the inherent insensitivity of magnetic resonance. In order to apply the new approach to biomedical applications, there is a need to develop experimental equipment, *in situ* quantification methods, and a biocompatible solvent. We present results detailing a low-field SABRE polarizer which provides well-controlled experimental conditions, defined spins manipulations, and which allows *in situ* detection of thermally polarized and hyperpolarized samples. We introduce a method for absolute quantification of hyperpolarization yield *in situ* by means of a thermally polarized reference. A maximum signal-to-noise ratio of $\sim 10^3$ for 148 μmol of substance, a signal enhancement of 10^6 with respect to polarization transfer field of SABRE, or an absolute ^{1}H-polarization level of $\approx 10^{-2}$ is achieved. In an important step toward biomedical application, we demonstrate ^{1}H *in situ* NMR as well as ^{1}H and ^{13}C high-field MRI using hyperpolarized pyridine (d_3) and ^{13}C nicotinamide in pure and 11% ethanol in aqueous solution. Further increase of hyperpolarization yield, implications of *in situ* detection, and *in vivo* application are discussed.

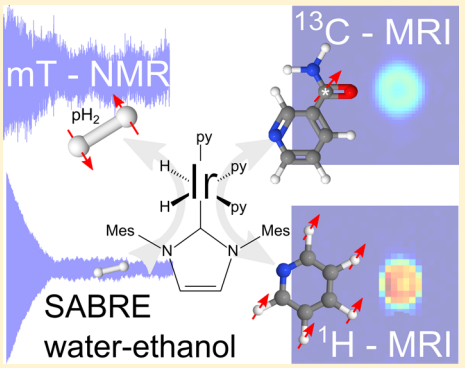

Magnetic resonance (MR) is an invaluable tool which finds application in many research fields despite its inherent insensitivity. This situation holds true even when employing the strongest available superconducting magnets which exceed the earth's magnetic field strength by 100 000 times. This is because only a miniscule fraction of the nuclear spins present in a sample contribute positively to the detected MR response when their alignment is thermally controlled. For the most commonly analyzed spin, ^{1}H (spin $^1/_2$), this is, in effect, the population difference that exists across addressable spin states and amounts to only 3 spins per million per Tesla (T). The situation is far worse for all other stable nuclei because their interactions with the magnetic field are even weaker. As a consequence, while NMR is an essential tool in the analytical chemist's arsenal, there is a significant need to improve the detection limits which will open up many new areas of analysis and diagnosis.

Hyperpolarization (hyp) methods can be used to address the poor thermal distribution of spins and have been discussed and employed for some time. Common sources of such hyperpolarized spin order include polarized light,[1−4] electron spin,[5−8] and *para*hydrogen (pH$_2$).[9−15] Dynamic nuclear polarization (DNP) is currently one of the most frequently used methods, due to its flexibility in hyperpolarizing a wide range of molecules as well as its commercial availability and well-developed experimental approach.

Utilization of pH$_2$, the nuclear spin-singlet of dihydrogen, was suggested as a potential route to MR signal enhancement in the 1980s, where "pH$_2$ and synthesis allow dramatically enhanced nuclear alignment" (PASADENA), "pH$_2$ induced polarization" (PHIP), and "adiabatic longitudinal transport after dissociation engenders net alignment" (ALTADENA) reflect the early approaches.[9−12] These methods rely on adding the spin order of a single pH$_2$ molecule into a target dihydrogen acceptor, by means of hydrogenation.

A wide range of studies have been reported that use this approach to probe catalysis[16−18] and support biomedical *in vivo* imaging.[19−23] Some of these results have employed polarization transfer to longer-lived ^{13}C nuclei by means of *r.f.* sequence application.[14,24] The quality control and equipment necessary for *in vivo* experimentation has been described, but the technique is not yet available as a "push-button" method.[25−28]

Received: November 11, 2013
Accepted: January 7, 2014
Published: January 7, 2014

   dx.doi.org/10.1021/ac403653q | *Anal. Chem.* 2014, 86, 1767−1774

Recently, the detection and quantification of ^{13}C-polarization achieved via such a transfer at a B_0 field of ≈50 mT[29] and steps toward a catalyst-free pH_2-hyperpoalrization[30] was presented and this can be considered as an important step in moving toward routine and reliable biomedical application.

In 2009 it was demonstrated that pH_2 does not need to actually be incorporated into the target. Instead, pH_2 and a substrate were brought into reversible interaction at a metal center. When this process occurs in an appropriate magnetic field, B_S, strong hyperpolarization is observed and this was termed SABRE.[31,32] SABRE stands for signal amplification by reversible exchange and, although a method in its infancy, its potential to achieve rapid hyperpolarization has resulted in significant research interest. Published work has focused thus far on demonstrating its potential for chemical analysis.[33−35] Typically, SABRE has been reported to occur in a methanol solution, after shaking a sample to introduce pH_2 in a stray field (~5 × 10^{-3} T). Upon transfer into a high-field magnet, hyperpolarized signals have been observed in the free substrate. This process is illustrated in Figure 1, which demonstrates the simplicity of SABRE. Methanol, however, is neither biocompatible nor suited for *in vivo* measurements.

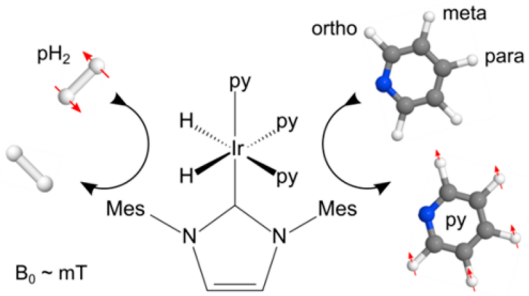

Figure 1. Schematic of SABRE: The pure and NMR-invisible spin order of pH_2 is transferred into observable hyperpolarization of the pyridine (py) target during their temporary contact, in low field, mediated by the metal complex. The red arrows indicate how spin-order equilibration leads to hyperpolarization in the ortho-, meta- and para-^{1}H-nuclei of the free pyridine receptor.

Accurate experimental conditions, the absolute quantification of the level of hyperpolarization *in situ*, and biocompatible solvents are important milestones for SABRE toward biomedical application, which have not yet been addressed in the literature. In this contribution, we will detail the following: (i) a SABRE polarizer which provides well-controlled experimental conditions and enables reproducible and repeatable *in situ* detection in various solvents, (ii) a method for absolute quantification of *in situ* hyperpolarization at low field, and also following transfer to high field, and (iii) NMR of SABRE hyperpolarized pyridine at Earth-, SABRE-, and high-field, as well as MRI of ^{13}C-nicotinamide in pure ethanol and an ethanol−water mixture.

MATERIALS AND METHODS

***Para*Hydrogen.** pH_2 with a purity of >95%, as described elsewhere, was used in this study.[36] A volume of 3 L of pH_2 at a pressure of ≈35 bar was produced and stored in an aluminum cylinder prior to completion of SABRE.

Chemistry. The SABRE catalyst reported[37] and recently investigated further[38] Ir(1,5-cyclooctadiene) (1,3-bis (2,4,6-trimethylphenyl) imidazolium) Cl (MW = 639.67 g/mol) was employed to polarize pyridine (py, MW = 79.1 g/mol, Carl Roth, Germany). Catalyst and substrate were dissolved in (a) 99.8% methanol-d_4 (Carl Roth, Germany), (b) 100% ethanol (Sigma-Aldrich), or (c) 100% ethanol followed by dilution with water in the ratio 1:9.

^{13}C-Nicotinamide Route 1. ^{13}C-nicotinic acid (744 mg, 6 mmol) was added to $SOCl_2$ (2 mL) heated to 80 °C for 2 h and then allowed to cool. The excess $SOCl_2$ was removed *in vacuo*, and the resulting acid chloride was added dropwise to a cooled (0 °C) conc. ammonia solution (5 mL). The solution was subsequently concentrated *in vacuo* and the crude product purified via column chromatography (10% MeOH in DCM) to afford the product as an off-white powder (280 mg, 38%).

^{13}C-Nicotinamide Route 2. From methyl-^{13}C-nicotinoate, 600 mg, 3.89 mmol was added to a solution of MeOH (5 mL) and conc. ammonia solution (5 mL), and the reaction stirred for 18 h at 20 °C. The solution was subsequently concentrated *in vacuo* and the crude product purified via column chromatography (10% MeOH in DCM) to afford the product as an off white powder (362 mg, 76%).

^{1}H NMR (400 MHz, CD_3OD): 8.99 (app. td, J = 2.3, 0.9 Hz, 1H), 8.66 (ddd, J = 5.0, 1.7, 0.6 Hz, 1H), 8.26 (dddd, J = 8.0, 3.9, 2.3, 1.7 Hz, 1H), 7.51 (app. ddt, J = 8.0, 5.0, 0.8 Hz, 1H). ^{13}C NMR (101 MHz): 170.0 (^{13}C), 153.0 (d, J = 0.6 Hz), 149.6 (d, J = 3.5 Hz), 137.5 (d, J = 2.1 Hz), 131.6 (d, J = 63.4 Hz), 125.3 (d, J = 3.3 Hz). MS (ESI) m/z (rel.%): 124 $[M + H]^+$ (100), 85 (24), 61 (24). HRMS (ESI) calculated for $^{13}C^{12}C_5H_7N_2O$, 124.0586; found, 124.0590.

The synthesis of 3,4,5-trideuterio-pyridine extends upon a route described by Cowley et al.[37] and Pavlik et al.[39]

***In Situ* and Field-Cycling Polarizer.** The solution composed of solvent, catalyst, and substrate was placed in a reaction chamber that was manufactured from polysulfone and withstands a pressure of 15 bar (Figure 2b,c, length 8 cm, radius

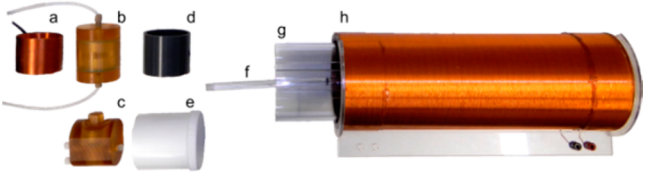

Figure 2. Experimental equipment used for *in situ* SABRE hyperpolarization and quantification: (a) low-field transmit and receive coil (f_0 ≈ 230 kHz), (b,c) typical reaction chambers, (d,e) reaction chamber holders, (f,g) mixing device, (h) electromagnet used to establish a uniform and well-defined polarization transfer field B_S.

2.75 cm, inner volume 13.3 mL).[27] PTFE tubing was connected to the ports of the reaction chamber to allow pH_2 injection, gas venting, and solution transfer, controlled by electromagnetic solenoid valves. The chamber was placed into the low-field NMR or Earth's field cycling setup as described below. To allow shaking of the chamber, a vortexer was placed outside of the B_0 coil and connected to the reaction chamber's holder (Figure 2d,e) using an acrylic rod.

In Situ Low-Field NMR. We modified the recently presented prototype for NMR at very low fields[40] for quantitative *in situ* detection of thermally and hyperpolarized samples. A static magnetic field was generated by the illustrated, numerically optimized, resistive solenoid (Figure 2h, length 35 cm, radius 6 cm, two layers of copper wire r = 0.5 mm, additional windings on the ends to improve homogeneity). Simulations predicted a

dx.doi.org/10.1021/ac403653q | *Anal. Chem.* 2014, 86, 1767−1774

very high level of homogeneity within the area of the reactor as the difference between B_{max} and B_{min} is only ≈8.6 × 10^{-7} T. The magnet was powered by a low-noise battery-driven current controller.[40]

For signal excitation and detection, a solenoid transmit-receive coil was constructed to fit around the reaction chamber. (Figure 2a,b, f_0 ≈ 230 and 270 kHz, 2.75 cm radius, 4.4 cm length, 280 μm wire diameter, capacitance 390 pF). Crossed diodes were added in the transmission path for rapid passive switching between transmission and receive. Excitation pulses were generated using a digital-to-analog converter controlled by custom software (6251 USB, National Instruments and Matlab, The Mathworks). The NMR signal was detected in the same device, 1−2 ms after excitation.

The ^{1}H NMR flip angle was adjusted as optimized signal from deionized water at thermal equilibrium and 5.4 mT. The resulting flip-angle error is estimated to 1°.[40] The experimentally observed line widths vary between 10 and 45 Hz, likely depending on the filling of the reactor. For SABRE, the reaction chamber was held in the center of the magnet and was connected to a commercial vortexer (Figure 2d,f) which allowed for efficient gas mixing (optionally).

Field-Cycling NMR. Flip angles and field homogeneity of the field-cycling NMR and MRI unit (Terra-Nova, Magritek, NZ) were adjusted according to the MR signal of a water sample that was prepolarized for 4 s at 20 mT. For hyperpolarization experiments, fresh pH_2 was supplied for every acquisition to the headspace of the reaction chamber (Figure 2c). The SABRE process was established under a transfer field, B_S, that could be set between 0.5 and 24 mT and held constant for 4 s. The B_S field was then turned off and the sample interrogated by a simple 90°-pulse-acquisition experiment in the shimmed Earth's field at ≈2.1 kHz (50 μT). In view of the fact that there is a need to prepolarize the nonhyperpolarized reference sample, an absolute quantification of the hyperpolarized signal cannot easily be made in such a field cycling device.

High-Field MRS and MRI. A glass vial was filled with water and placed in the MRI or NMR system for calibration (two Biospec, 70/20 Avance III for ^{1}H MRS and ^{13}C MRI or 400 MHz, 89 mm vertical bore DRX for ^{1}H MRI, Bruker, Germany). For SABRE, an appropriate solution was placed into the vial and sealed. pH_2 was introduced into the solution through either a Young's valve or a syringe needle. After ≈10 s in a field of between 1 and 6.5 mT, the sample was introduced into the high-field magnet and either nonlocalized spectra or MRI data were recorded within seconds.

All proton images were acquired using the RARE pulse sequence,[41] a single-shot method which allows for acquisition times shorter than or of the order of 1 s. For the pyridine and pyridine-d_3 images, methanol-d_4 was employed as the solvent and the acquisition parameters used were echo time (TE) 7.5 ms, field of view (FOV) 40 mm × 40 mm, slice thickness 2 mm, and acquisition matrix 64 × 64. The associated parameters used to collect the ^{13}C-nicotinamide image reported here in methanol or ethanol solution were TE 7.5 ms, FOV 6 cm × 6 cm, slice thickness 30 mm, and acquisition matrix 32 × 32, zero-filled to 128 × 128.

Quantification Methods. High-field data were processed using the manufacturer's Paravision and Topspin package and Matlab. The signal enhancement (η) and absolute polarization yield (P_{hyp}) for spectra was quantified by comparing the integral of the hyperpolarized signal S_{hyp} to the signal in thermal equilibrium S_{therm} of the sample, acquired with identical parameters as shown in eq 1. For imaging, if the thermal signal of the nonhyperpolarized sample was too low for direct detection, the signal of a second sample was used as reference. However, quantification of the absolute hyperpolarization yield is exacerbated by relaxation weighting of the sequence and different relaxation properties of sample and reference. Thus, in this work, we report an apparent enhancement of contrast instead of absolute signal enhancement.

$$\eta_{hyp}(\text{high field}) = \frac{S_{hyp}(\text{Py})\cdot \text{NEX}_{therm}}{S_{therm}(\text{Py})}$$

$$P_{hyp}(\text{high field}) = \eta \cdot P_{therm}(^1\text{H, 7 T}) \quad (1)$$

where P_{therm} (^{1}H, 7T) = 2.5 × 10^{-5}.

A similar problem presents itself for low-field NMR. It was pointed out before that direct detection of MR signal at ≈10^{-3} T in a single acquisition is not possible but requires prepolarization at much higher fields, as only 3 ppb of all spins effectively contribute to the signal.[42] Only recently, we presented the detection of a thermally polarized MR signal at 10^{-3} T after a single excitation.[40] The apparatus described here improves on this by using reaction chambers and exploiting dedicated transmit-receive coils fitted to the chamber. Even with this equipment, however, the amount of nonhyperpolarized substrate is far too low for its direct detection. Under these conditions, the level of hyperpolarization was quantified by reference to the thermal signal of a 0.74 M H_2O sample. Of the 1.48 mol of protons in this sample, $^1/_4$ are invisible as they are in the para-state[43] and do not contribute to the signal. Consequently, the signal arises for an effective 1.1 mol of protons. Area, line width, and peak height data were obtained by fitting a Lorentzian function to the detected low-field resonances (Matlab). The signal-to-noise ratio (SNR) was calculated by dividing the height of the resonance at 230 kHz by the standard deviation of the data between 216 and 228 kHz.

The area of the H_2O reference spectrum in Figure 3 was quantified as 104.7 au (NEX = 10 free-induction decays, TR = 15 s, α = 90°, T_1 (H_2O, 5.4 mT) ≈ 2.7 s). The summed spectra, and the mean of the individual spectra, exhibited a $SNR_{NEX=10}$ of 88.9 and $SNR_{NEX=1}$ of 31.4, respectively. Thus, in thermal equilibrium at this field, the limit of detection (SNR = 2) was ≈70 mmol of water protons, which corresponds to about 1 nmol of polarized spins.

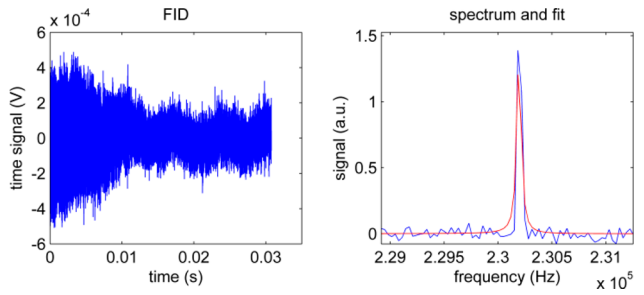

Figure 3. Low-field ^{1}H-NMR reference signal of H_2O used for quantification of the ^{1}H-hyperpolarization yield. Sum of 10 free induction decays (left) and real spectrum with fit (right) of 0.74 mol of deionized H_2O detected in thermal equilibrium at B_0 = 5.4mT (TR = 15 s, fwhm = 45 Hz, SNR = 89).

dx.doi.org/10.1021/ac403653q | Anal. Chem. 2014, 86, 1767−1774

The associated full-width at half-maximum (fwhm) of the line of the H_2O sample were $fwhm_{NEX=10}$ = 45 Hz and $fwhm_{NEX=1}$ = 42 Hz, respectively. These data demonstrate a near stable field homogeneity throughout the experiment, which accounts for the 10% lower than expected SNR increase.

The ^1H polarization in thermal equilibrium at 290 K is 1.90×10^{-8} at 5.4 mT. This leads to the following equations for signal enhancement (η) and absolute polarization yield (eq 2).

$$\eta_{hyp}(\text{low field}) = \frac{S_{hyp}(Py)}{S_{therm}(H_2O)} \cdot \frac{NEX_{therm}(H_2O)}{NEX_{hyp}(Py)} \cdot \frac{n_A(^1H)}{n_A(Py)}$$

$$P_{hyp}(\text{low field}) = \eta \cdot P_{therm}(^1H, 5.4\ \text{mT}) \quad (2)$$

where S_{hyp} and S_{therm} are the area of hyperpolarized and thermally polarized resonances, NEX is number of excitations, and n_A is the amount of substance.

At 5.4 mT, a 45 Hz line-width equates to ≈200 ppm, which is now 2 orders of magnitude above the typical chemical shift range of ^1H resonances. Consequently, the ^1H resonances for all molecules are collapsed into one peak during these measurements. In the case of SABRE-derived magnetization in low field, the single line is comprised of all the coherence order created by the simple excitation pulse. Thus, even though significant polarization can be detected, it cannot be attributed to an individual proton resonance. Furthermore, any variation in phase across proton resonances, as is typical in SABRE or PHIP, may cancel a portion of the detected signal. The hyperpolarization level achieved for pyridine is therefore reported per molecule as a whole, which holds five protons. The enhancement of each of these hydrogen nuclei is known to vary in high field, in both phase and magnitude, but are treated equally here because we cannot resolve such effects in low field.

RESULTS

***In Situ* Detection and Quantification at Low Field in Methanol.** When a thermally polarized 148 μmol sample of pyridine in 4.7 mL of methanol-d_4 and 2 mM catalyst was monitored at 5.4 mT, no ^1H signal is observed, as was expected. However, when pH_2 was utilized to activate the SABRE effect, a substantial signal was observed indicative of strong enhancement. The SNR achieved for the data in Figure 4 that was collected with one acquisition was 1.67×10^3. Compared to the fitted peak area of a H_2O reference, a signal enhancement value, η_{hyp} of 320×10^3 was estimated. This corresponds to an absolute polarization level of ≈0.6% (eq 2) and confirms that low concentration analytes can be readily detected through SABRE even at low field.

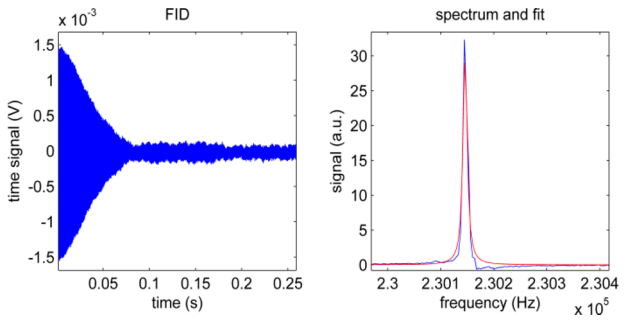

Figure 4. Representative low-field ^1H-NMR time-domain data, spectrum and fit obtained *in situ* for 148 μmol of SABRE hyperpolarized pyridine in 4.7 mL of CD_3OD in the presence of 2 mM catalyst at 5.4 mT with a SNR of 1.6×10^3 confirming that low concentration analytes can be observed in a single acquisition.

***In Situ* Detection and Quantification at Low Field in Pure and Diluted Ethanol.** A strong signal was also observed when this enhancement method was applied to 35 mg of pyridine and 14 mg of catalyst dissolved in either 4 mL of ethanol or 9:1 H_2O–ethanol mixture. In these cases, polarization levels of 0.2 and 0.02%, respectively, were achieved *in situ* (Figure 5). These correspond to signal enhancement, η_{hyp},

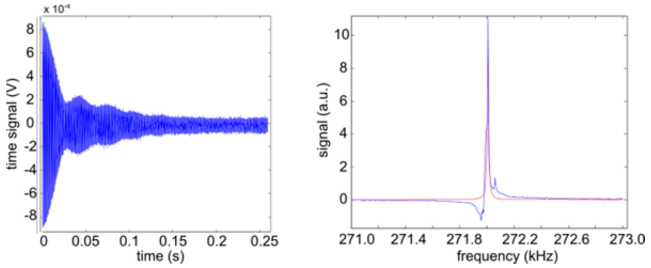

Figure 5. Low-field ^1H NMR time-domain data, spectrum, and fit of hyperpolarized Py in 4 mL of 9:1 water–ethanol mixture *in situ* at 6.3 mT. The irregular line shape may be attributed to inhomogeneities associated with the injection of pH_2.

values of between 10^4 and 10^5. No difference was observed if the catalyst was activated with H_2 before or after the addition of water, nor when the amount of ethanol was reduced to 0.4 mL, which, after dilution, may be considered an important first step toward SABRE-hyperpolarized *in vivo* MRI.

As stated above, the single resonance observed in Figures 4 and 5 reflects the sum of the contributing SABRE hyperpolarization from all individual proton sites. A fifth of the polarization may be attributed to each.

Chemical Shift Resolution at High Field. To shed light on the phase distribution, we have acquired high-field spectra. We seek here to compare measurements at low and high field and consider how changes from the transfer field, B_S, (of order 10^{-3} T) to the measurements fields affects the results.

When the analogous SABRE-polarized sample consisting of 5.8 mg of catalyst, 11.8 mg of Py in 4.2 mL of methanol-*d*4 was transferred to high field, chemical-shift resolved signals for the three distinct proton sites of pyridine were observed that show phase variations according to the transfer field B_S. These data are reproduced in Figure 6.

The highest hyperpolarization yield was detected when the mixing B_S field was between 4 and 7 mT. In this region, all the detected high field signals are in phase. It is also possible to sum the associated signal intensities to estimate what might be observed in low field. The data obtained via this route are indicated in Figure 7 by circles, which suggest that the optimum polarization transfer field is the similar regardless of where the measurement is made. Note, though, that the sample experienced fields ranging from $B_S \approx 10^{-3}$ T during SABRE, $B_{transfer} \approx 10^{-5}$ T during transfer, and $B_{detection} \approx 10^{1}$ T at detection.

Solvent Effects Monitored by *in Situ* Detection at Low Field. A more precise measure of the effects due to field change was estimated by using the field-cycling system. In this apparatus, the sample experiences less field variations as no transfer is necessary, namely, an initial field of $B_S \approx 10^{-3}$ T for

dx.doi.org/10.1021/ac403653q | Anal. Chem. 2014, 86, 1767–1774

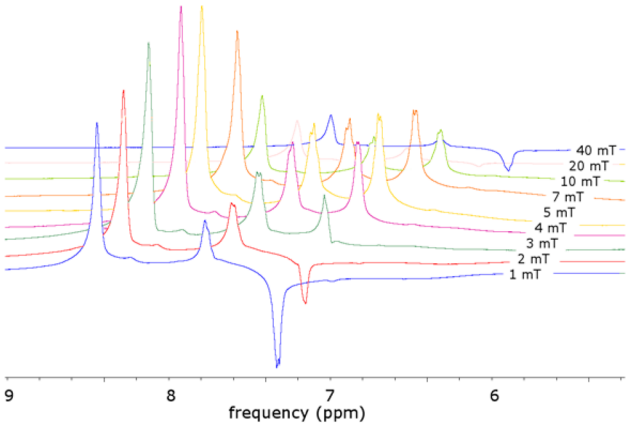

Figure 6. ^{1}H-NMR spectra of hyperpolarized pyridine in methanol-d_4 acquired on a 7 T MR imager, polarized at low field over a range of B_S = 1−40 mT. The spectra were integrated with the phase as shown and plotted as circles in Figure 7

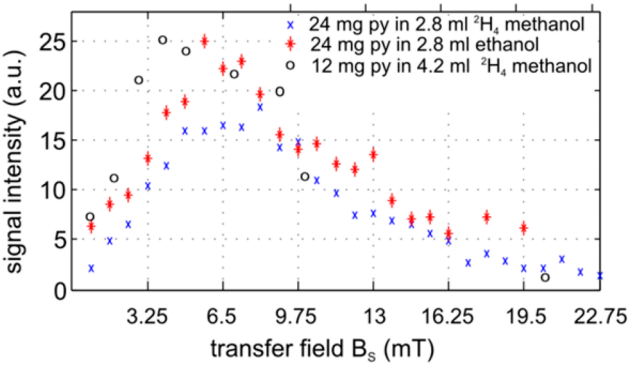

Figure 7. Signal intensities of hyperpolarized pyridine in methanol-d_4 and ethanol as a function of the transfer field, B_S, over the range 0.5−22 mT. Signals were detected at Earth field (× and ∗) or at 7 T (○). The latter were scaled to the same maximum value.

SABRE and $B_{detection} \approx 10^{-5}$ T for detection. B_S was varied between 0 and 22.75 mT and the resulting data is displayed in Figure 7, along with the integrals of the high-field spectra as described in the previous section, scaled to fit. The signal maxima for SABRE in methanol and ethanol occur with very similar B_S-field values. When the rates of magnetization build-up are considered as a function of the duration of the B_S period for each solvent, the signals in ethanol were found to appear with twice the growth rate of those in perdeuterated methanol at 4 and 8 s, respectively. These time constants describing the polarization build-up indicate that the maximum polarization is not achieved while the transfer field B_S is applied for 4 s. A total of 9 mg of catalyst were used.

Enhanced Polarization through Isotopic Substitution. Because of the fact that pyridine has three magnetically nonequivalent protons, three separate enhanced resonances were identified in high-resolution liquid-state ^{1}H NMR spectra in CD_3OD, located at 8.5, 7.8, and 7.4 ppm, respectively. While this may represent an advantage in some cases, as it allows for an in-depth investigation of the influence of the mixing field on the enhancement at various sites (see previous section), it raises significant difficulties when pyridine is used in imaging experiments. Not only is the magnetization transferred to several protons, leading to relatively low average polarization levels in an image, but the fast relaxation rates and the chemical shift artifacts which arise from the presence of nonequivalent nuclei, further lower the results' quality and contrast.

In order to circumvent this situation, pyridine-3,4,5-d_3 was prepared. Pyridine-3,4,5-d_3 presents the obvious advantage that the magnetization is transferred to the only remaining two (equivalent) ortho-protons, which furthermore have slower relaxation rates compared to the nondeuterated molecule of 31 s in methanol-d_4.

2D magnetic resonance imaging data of milligrams of hyperpolarized pyridine and hyperpolarized pyridine-d_3, respectively, in 0.6 mL of CD_3OD and 2 mg of catalyst were acquired in order to illustrate the strong effect isotopic substitution can have on the signal.

A 169-fold apparent contrast enhancement was calculated based on a H_2O internal standard for the image of the sample containing pyridine (Figure 8, top). When analyzing the images acquired on the sample prepared with deuterated substrate, upon comparison with the reference sample, a contrast enhancement η_{hyp} of 807 was obtained. This enhancement

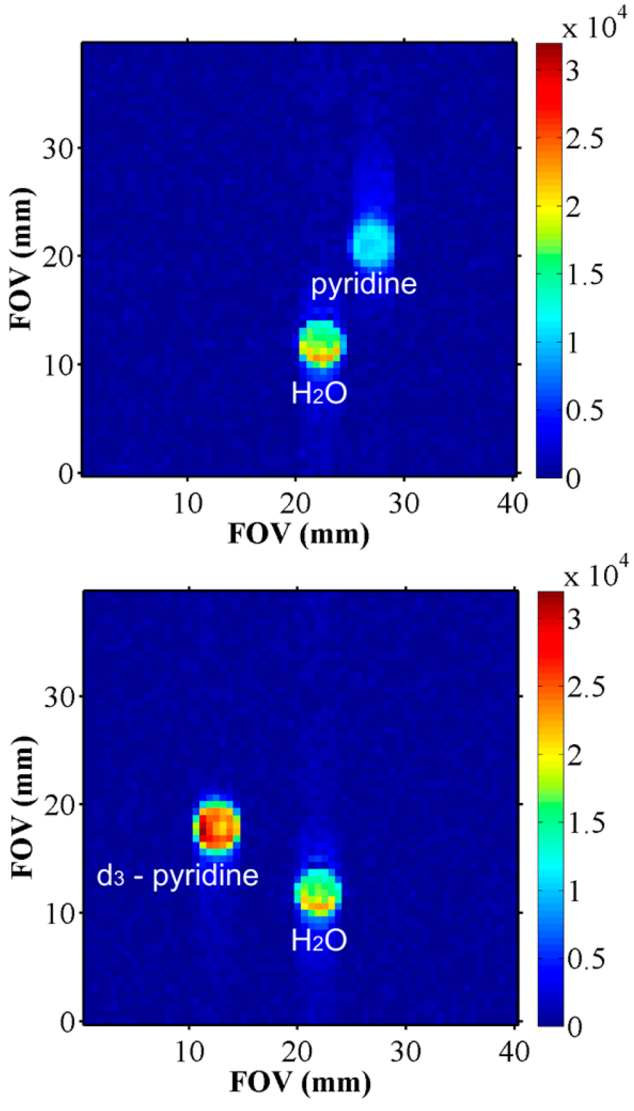

Figure 8. ^{1}H-RARE image of hyperpolarized pyridine (top) and pyridine-3,4,5-d_3 (bottom), each with a reference sample, dissolved in methanol and acquired at 9.4 T. A stronger signal was observed from SABRE when the deuterated substrate was used.

dx.doi.org/10.1021/ac403653q | *Anal. Chem.* 2014, 86, 1767−1774

corresponded to an apparent polarization level of 2.5% (Figure 8, bottom). The associated increase in polarization level is due to the more efficient transfer of magnetization during SABRE to fewer proton sites in 3,4,5-d_3-pyridine and the longer T_1 value for the remaining two protons.

High-Field ^{13}C-Imaging of SABRE-Derived Signals. Given the established utility of exploiting the long T_1 of ^{13}C by *in vivo* DNP and PHIP, we have also investigated the hyperpolarization of a ^{13}C in a carbonyl group using SABRE. This involved the initial preparation of a sample of ^{13}C-enriched nicotinamide. The resulting ^{13}C-MRI of hyperpolarized nicotinamide that was detected in a single acquisition where P_{hyp} is 0.03% is shown in Figure 9. Solution volumes were 0.6 mL methanol-d_4 with 2 mg of catalyst and 5 mg of substrate.

DISCUSSION

In this paper we investigated the intricacies of SABRE hyperpolarization in a wide range of fields, at $\approx 10^{-3}$ T *in situ*, at $\approx 10^{-5}$ T in the Earth' field, and at $\approx 10^{1}$ T in the high fields of superconducting magnets. Furthermore, we investigated biocompatible solvents and demonstrated high-field ^{1}H and ^{13}C MR imaging of isotopically enriched substances with respect to an *in vivo* application.

We have shown that a recently developed low-field MR system allows *in situ* signal detection and quantification by means of using a thermally polarized reference. This has enabled us, for the first time, to monitor and quantify the SABRE hyperpolarization yield at B_S, the point of polarization transfer. It has been shown that in the case of pyridine a signal enhancement value η_{hyp} of 320×10^3 results which equates to $\approx$0.6% ^{1}H polarization and is sufficient for MRI detection. To generate an equal polarization in thermal equilibrium at room temperature, a magnetic field of $\approx$3000 T would be required.

While this represents a signal enhancement of 6 orders of magnitude compared to B_S, it is still two orders below unity. Higher pressure or other means to increase the pH_2 concentration in solution may be used to increase the hyperpolarization yield further. This is supported by preliminary findings that the hyperpolarization yield increased $\approx$2.5-fold by doubling the pH_2 pressure from 5 to 10 bar. Given the lower solubility of H_2 in H_2O, which is roughly 0.8 mM compared to 4 mM in methanol at 1 bar and room temperature, we expect this to be very important in studies using water.

The *in situ* detection approach offers several advantages over the conventional high-field detection methods which necessarily involve sample transport and hence a delay where relaxation can occur. There is also the possibility of further spin state evolution during the transfer process which typically takes several seconds. The data presented here suggest that such effects do not strongly affect the optimal field for SABRE, B_S, for the compound investigated. What is clear, however, is that there is no need to fully commit an expensive instrument to developing this phenomenon, as many important observations can be made at low field without chemical shift resolution (e.g., new agents or catalysts). Furthermore, interesting low-field application may emerge.

Many of the molecules SABRE hyperpolarizes contain nonequivalent nuclei. In order to observe the relative signal amplitudes that result from the probing of these environments, separate resonances are required. As Figure 6 reveals, these effects can be substantial. Figure 7, however, shows that both *in*

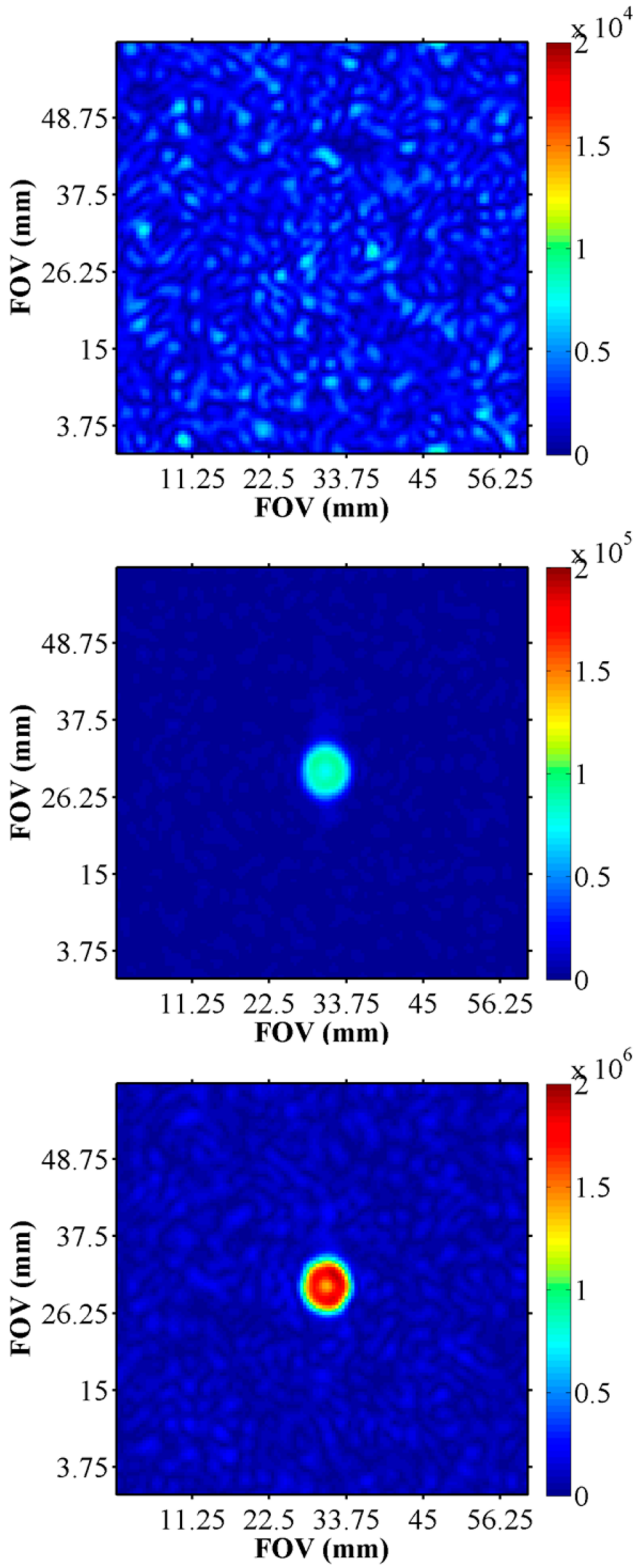

Figure 9. Single-acquisition ^{13}C-RARE MRI at 7 T of a 8 mm diameter phantom containing ^{13}C-labeled nicotinamide in methanol-d_4, before (top) and during hyperpolarization using the SABRE method (middle). Both images took approximately 1 s to acquire. Bottom: Comparative image of the sample in thermal equilibrium collected with 1100 averages that took 18 h 20 min used to establish the level of ^{13}C signal enhancement was 65-fold, corresponding to a polarization of 0.03%.

dx.doi.org/10.1021/ac403653q | *Anal. Chem.* 2014, 86, 1767−1774

situ and high-field detection provide a similar view of the effect B_S plays on the overall signal response of pyridine. The advantage of an in-phase signal was pointed out before[32,44] and is being investigated.

When pyridine is examined using NMR imaging, significant artifacts may arise due to the multiple frequency responses. This problem is not present at low field, where the signals overlap due to the smaller frequency range over which the chemical shift is dispersed. However the net signal amplitude which is detected must be reduced due to internal cancellation as reflected in Figure 6. A strategy that overcomes internal cancellation is provided by deuteration and the examination of pyridine-3,4,5-d_3 or other single-resonance molecules. In this case, as the SABRE effect transfers spin-polarization into just two protons on pyridine, rather than the more usual five, and their relaxation time is extended, superior signal gains and hence better images are obtained in a very short amount of time.

A similar situation where a single resonance is detected is illustrated by using the biomolecule ^{13}C-nicotinamide. This molecule readily yields a ^{13}C-MR image through SABRE, albeit the polarization level is relatively low. Now as the T_1 of ^{13}C nuclei are longer than ^{1}H and no thermal background is visible, ultrafast *in vivo* imagining can be facilitated using this approach.

The key requirement for *in vivo* measurements of SABRE, however, is a biocompatible solvent, which is illustrated here in conjunction with ethanol and ethanol−water mixtures, where further dilution is possible. This route may be necessary until water-soluble catalysts are developed that deliver high polarization.

CONCLUSION

By means of a dedicated experimental setup and reference to a thermally polarized sample, *in situ* detection and absolute quantification of SABRE hyperpolarization was achieved in methanol, ethanol, and aqueous ethanol. ^{1}H and ^{13}C NMR imaging of hyperpolarized pyridine and ^{13}C-nicotinamide was demonstrated. Pure ethanol was found to be an efficient solvent for the catalyst, offering the perspective for first *in vivo* experiments in conjunction with biomolecules such as nicotinamide. *In situ* detection while SABRE takes place offers an interesting perspective of using renewing hyperpolarization.

These results demonstrate that no extensive hardware is required for highly sensitive NMR in aqueous solution. Because SABRE, unlike other hyperpolarization methods, does not necessitate extensive equipment and pH_2 may be stored for days to weeks, it may provide for mobile hyperpolarization on-demand. Its combination with portable, low-field MR systems[45] may open up new, previous inaccessible applications, including mobile diagnostic MRI or chemical analysis by NMR.

AUTHOR INFORMATION

Corresponding Author

*Address: Medical Physics, Dept. of Radiology, Breisacher Straße 60a, University Medical Center Freiburg, 79106 Freiburg, Germany. E-mail: jan.hoevener@uniklinik-freiburg.de.

Notes

The authors declare no competing financial interest.

ACKNOWLEDGMENTS

Jan-Bernd Hövener wishes to thank the Academy of Excellence of the German Science Foundation and the Innovationsfonds of Baden-Würtemberg. The Wellcome Trust (Grants 092506 and 098335) and the University of York are also thanked for supporting this work.

REFERENCES

(1) Bhaskar, N. D.; Happer, W.; McClelland, T. *Phys. Rev. Lett.* **1982**, *49*, 25−28.
(2) Ebert, M.; Grossmann, T.; Heil, W.; Surkau, R.; Leduc, M.; Bachert, P.; Knopp, M. V.; Schad, L. R.; Thelen, M. *Lancet* **1996**, *347*, 1297−1299.
(3) Albert, M. S.; Cates, G. D.; Driehuys, B.; Happer, W.; Saam, B.; Springer, C. S.; Wishnia, A. *Nature* **1994**, *370*, 199−201.
(4) Schröder, L.; Lowery, T. J.; Hilty, C.; Wemmer, D. E.; Pines, A. *Science* **2006**, *314*, 446−449.
(5) Hausser, K. H.; Stehlik, D. *Adv. Magn. Reson.* **1968**, *3*, 79−139.
(6) Abragam, A.; Goldman, M. *Rep. Prog. Phys.* **1978**, *41*, 395−467.
(7) Ardenkjaer-Larsen, J. H.; Fridlund, B.; Gram, A.; Hansson, G.; Hansson, L.; Lerche, M. H.; Servin, R.; Thaning, M.; Golman, K. *Proc. Natl. Acad. Sci. U.S.A.* **2003**, *100*, 10158−10163.
(8) Batel, M.; Krajewski, M.; Weiss, K.; With, O.; Däpp, A.; Hunkeler, A.; Gimersky, M.; Pruessmann, K. P.; Boesiger, P.; Meier, B. H.; Kozerke, S.; Ernst, M. *J. Magn. Reson.* **2012**, *214*, 166−174.
(9) Bowers, C. R.; Weitekamp, D. P. *Phys. Rev. Lett.* **1986**, *57*, 2645−2648.
(10) Bowers, C. R.; Weitekamp, D. P. *J. Am. Chem. Soc.* **1987**, *109*, 5541−5542.
(11) Eisenschmid, T. C.; Kirss, R. U.; Deutsch, P. P.; Hommeltoft, S. I.; Eisenberg, R.; Bargon, J.; Lawler, R. G.; Balch, A. L. *J. Am. Chem. Soc.* **1987**, *109*, 8089−8091.
(12) Pravica, M. G.; Weitekamp, D. P. *Chem. Phys. Lett.* **1988**, *145*, 255−258.
(13) Haake, M.; Natterer, J.; Bargon, J. *J. Am. Chem. Soc.* **1996**, *118*, 8688−8691.
(14) Goldman, M.; Johannesson, H. *C. R. Phys.* **2005**, *6*, 575−581.
(15) Chekmenev, E. Y.; Hövener, J.; Norton, V. A.; Harris, K.; Batchelder, L. S.; Bhattacharya, P.; Ross, B. D.; Weitekamp, D. P. *J. Am. Chem. Soc.* **2008**, *130*, 4212−4213.
(16) Duckett, S. B.; Mewis, R. E. *Acc. Chem. Res.* **2012**, *45*, 1247−1257.
(17) Duckett, S. B.; Wood, N. J. *Coord. Chem. Rev.* **2008**, *252*, 2278−2291.
(18) Green, R. A.; Adams, R. W.; Duckett, S. B.; Mewis, R. E.; Williamson, D. C.; Green, G. G. R. *Prog. Nucl. Magn. Reson. Spectrosc.* **2012**, *67*, 1−48.
(19) Golman, K.; Axelsson, O.; Jóhannesson, H.; Månsson, S.; Olofsson, C.; Petersson, J. s. *Magn. Reson. Med.* **2001**, *46*, 1−5.
(20) Hövener, J.-B.; Chekmenev, E. Y.; Harris, K. C.; Perman, W. H.; Tran, T. T.; Ross, B. D.; Bhattacharya, P. *Magn. Reson. Mater. Phys.* **2009**, *22*, 123−134.
(21) Bhattacharya, P.; Chekmenev, E.; Reynolds, W.; Wagner, S.; Zacharias, N.; Chan, H.; Bünger, R.; Ross, B. D. *NMR Biomed.* **2011**, *24*, 1023−1028.
(22) Zacharias, N.; Chan, H.; Sailasuta, N.; Ross, B. D.; Bhattacharya, P. *J. Am. Chem. Soc.* **2012**, *134*, 934−943.
(23) Trantzschel, T.; Plaumann, M.; Bernarding, J.; Lego, D.; Ratajczyk, T.; Dillenberger, S.; Buntkowsky, G.; Bargon, J.; Bommerich, U. *Appl. Magn. Reson.* **2012**, *44*, 267−278.
(24) Goldman, M.; Johannesson, H.; Axelsson, O.; Karlsson, M. *C. R. Chim.* **2006**, *9*, 357−363.
(25) Goldman, M.; Johannesson, H.; Axelsson, O.; Karlsson, M. *Magn. Reson. Imaging* **2005**, *23*, 153−157.
(26) Kadlecek, S.; Vahdat, V.; Nakayama, T.; Ng, D.; Emami, K.; Rizi, R. *NMR Biomed.* **2011**, *24*, 933−942.
(27) Hövener, J.-B.; Chekmenev, E.; Harris, K.; Perman, W.; Robertson, L.; Ross, B.; Bhattacharya, P. *Magn. Reson. Mater. Phys.* **2009**, *22*, 111−121.
(28) Agraz, J.; Grunfeld, A.; Cunningham, K.; Li, D.; Wagner, S. *J. Magn. Reson.* **2013**, *235*, 77−84.

(29) Waddell, K. W.; Coffey, A. M.; Chekmenev, E. Y. *J. Am. Chem. Soc.* **2011**, *133*, 97−101.
(30) Kovtunov, K. V.; Zhivonitko, V. V.; Skovpin, I. V.; Barskiy, D. A.; Salnikov, O. G.; Koptyug, I. V. *J. Phys. Chem. C* **2013**, *117*, 22887−22893.
(31) Adams, R. W.; Duckett, S. B.; Green, R. A.; Williamson, D. C.; Green, G. G. R. *J. Chem. Phys.* **2009**, *131*, 194505−194515.
(32) Adams, R. W.; Aguilar, J. A.; Atkinson, K. D.; Cowley, M. J.; Elliott, P. I. P.; Duckett, S. B.; Green, G. G. R.; Khazal, I. G.; López-Serrano, J.; Williamson, D. C. *Science* **2009**, *323*, 1708−1711.
(33) Lloyd, L. S.; Adams, R. W.; Bernstein, M.; Coombes, S.; Duckett, S. B.; Green, G. G. R.; Lewis, R. J.; Mewis, R. E.; Sleigh, C. J. *J. Am. Chem. Soc.* **2012**, *134*, 12904−12907.
(34) Glöggler, S.; Emondts, M.; Colell, J.; Müller, R.; Blümich, B.; Appelt, S. *Analyst* **2011**, *136*, 1566.
(35) Glöggler, S.; Müller, R.; Colell, J.; Emondts, M.; Dabrowski, M.; Blümich, B.; Appelt, S. *Phys. Chem. Chem. Phys.* **2011**, *13*, 13759−13764.
(36) Hövener, J.-B.; Bär, S.; Leupold, J.; Jenne, K.; Leibfritz, D.; Hennig, J.; Duckett, S. B.; von Elverfeldt, D. *NMR Biomed.* **2013**, *26*, 124−131.
(37) Cowley, M. J.; Adams, R. W.; Atkinson, K. D.; Cockett, M. C. R.; Duckett, S. B.; Green, G. G. R.; Lohman, J. A. B.; Kerssebaum, R.; Kilgour, D.; Mewis, R. E. *J. Am. Chem. Soc.* **2011**, *133*, 6134−6137.
(38) Weerdenburg, B. J. A.; van Glöggler, S.; Eshuis, N.; Engwerda, A. H. J. (Ton); Smits, J. M. M.; Gelder, R.; de Appelt, S.; Wymenga, S. S.; Tessari, M.; Feiters, M. C.; Blümich, B.; Rutjes, F. P. J. T. *Chem. Commun.* **2013**, *49*, 7388−7390.
(39) Pavlik, J. W.; Laohhasurayotin, S. *J. Heterocycl. Chem.* **2007**, *44*, 1485−1492.
(40) Borowiak, R.; Schwaderlapp, N.; Huethe, F.; Fischer, E.; Lickert, T.; Bär, S.; Hennig, J.; Elverfeldt, D.; Hövener, J.-B. *Magn. Reson. Mater. Phys.* **2013**, *26*, 491−499.
(41) Hennig, J.; Nauerth, A.; Friedburg, H. *Magn. Reson. Med.* **1986**, *3*, 823−833.
(42) Glöggler, S.; Blümich, B.; Appelt, S. *Top. Current Chem.* **2011**, 1−22.
(43) Carravetta, M.; Johannessen, O. G.; Levitt, M. H. *Phys. Rev. Lett.* **2004**, *92*, 153003-1−153003-4.
(44) Dücker, E. B.; Kuhn, L. T.; Münnemann, K.; Griesinger, C. *J. Magn. Reson.* **2012**, *214*, 159−165.
(45) Danieli, E.; Perlo, J.; Blümich, B.; Casanova, F. *Angew. Chem.* **2010**, *122*, 4227−4229.